# 10 Interactivity of decision mechanisms

In this chapter, we continue with our analysis of a specific two-strategy two-person game, the attack-defense game. Before proceeding, we acknowledge that even in the context of our specific *free fall* solution, there are many effects that interact with each other. We believe that this complexity reflects the reality of decision processes. As part of our work in this chapter, we shall attempt to isolate specific effects from this complexity and relate them to our common experiences. In the past, these effects have been ignored or treated as working independently.

Note that the advantage of a complete theory is that it provides an integrated view of these effects. We pointed out the importance of treating things globally in section 7.8 as a generic goal of modeling the social and economic behaviors. Our approach here is the same as the one described in that section. We look for stable behaviors and see how the system responds to stimuli. We ensure that our theory has "closed loops" so that all the interactions are captured. We build up our numerical model so that we can easily change our assumptions about initial values to consider other cases or sensitivity analysis on the current case. Though not required, it is suggested that the reader carry out the calculations described in the exercises at the end of the chapter to build up an intuition of the interactivity of the many effects incorporated into the theory. We start with the role of payoffs in the theory.

## 10.1 *Payoffs*

One interesting set of behaviors is generated directly from the payoffs for "Blue" (Figure 10-1) and "Red" (Figure 10-2) as well as the payoff for the *code of conduct behavior* that they share. Taking only the game theory relevant values, we would get less richness, though we do start with Eq. (8.62) for the initial payoff values without the "dot" approximations. For these plots we have assumed the *ownership model* and assumed that each player takes on a certain passion $\mathbf{P}_\alpha$. We assume that the initial passion components are not zero:

$$P_\alpha(x,y,0)=\left\{4\cos^2\frac{\pi x}{10},\quad -4\cos^2\frac{\pi y}{10},\quad 2\cos^2\frac{\pi x}{10}\cos^2\frac{\pi y}{10}\right\} \tag{10.1}$$

We have picked these numbers to show that they make a difference in the outcome payoffs. From the payoff figures we see that away from the *still point*, each force demonstrates a dramatically different form. Each passion gradient (Figure 10-3 and Figure 10-4) acts like a current that generates the payoffs, though there are other effective currents that influence the outcomes.

We have chosen the boundary conditions in such a way that "Blue" correctly "owns" $x$, "Red" correctly owns $y$ and the code of conduct player can own both. In other words, though the behaviors are not physical currents, there are similarities in their behavior that lead to similar consequences to analogous fields. This is an example where the mathematics is the same though the underlying processes are not. It is also another example of non-game theory factors such as passion having a role in the decision process. We think of passion as an external influence that can "generate" a payoff as opposed to taking the payoffs as simply given as an externally specified set of rules.

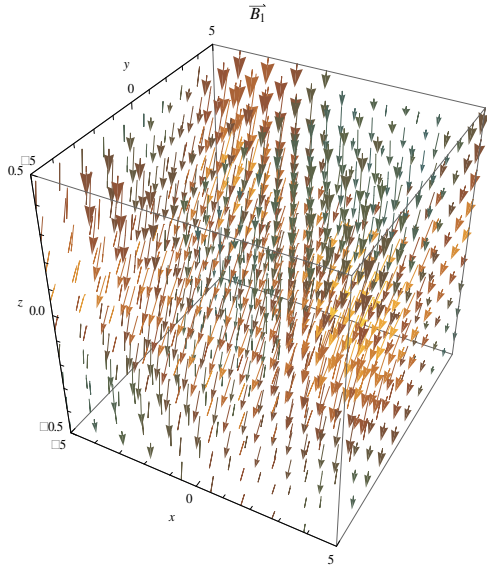


**Figure 10-1: Attack defense "Blue" payoff $\mathbf{B}_1$**

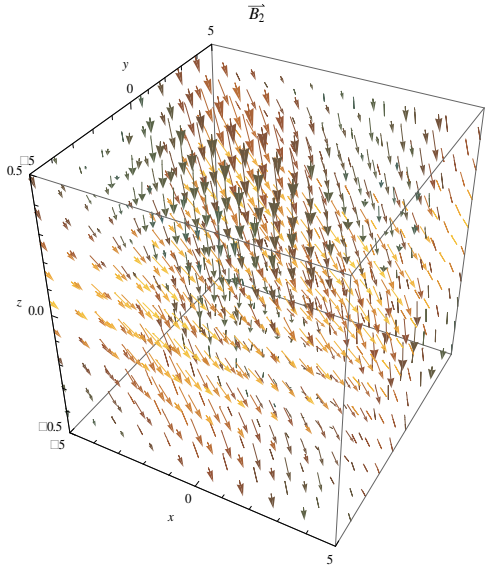


**Figure 10-2: Attack defense "Red" payoff $\mathbf{B}_2$**

Based on our field equations, we expect that the *composite payoff* vector will be the weighted average of the player payoffs with the engagement factors. Since the "Blue" and "Red" engagement factors grow, we expect to see the effects of this average. We will have to moderate our expectations based on the effects of the gauge factor.

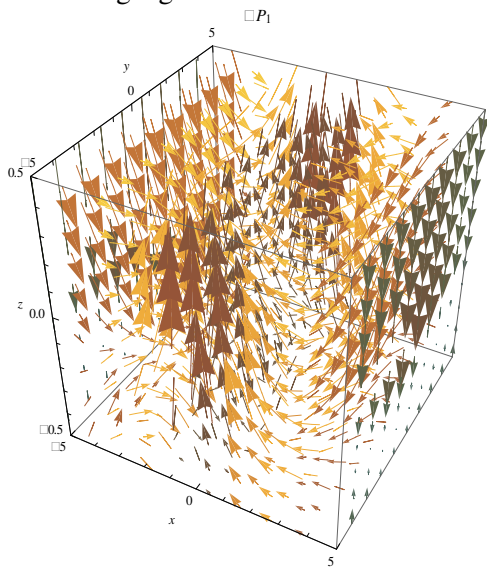


**Figure 10-3: "Blue" passion gradient $\mathbf{P}_1 = \nabla P_1(x, y, z)$**

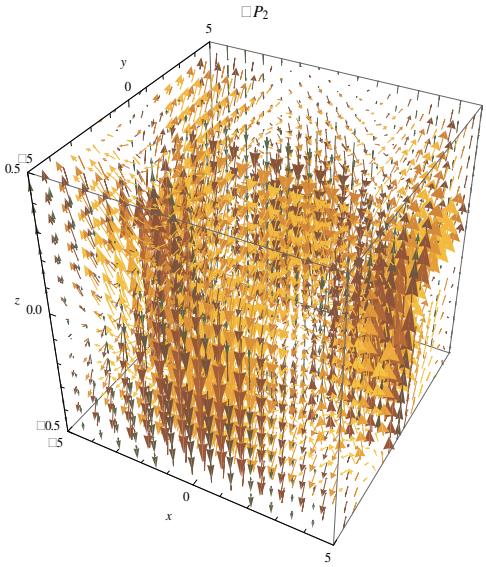


**Figure 10-4: "Red" passion gradient $\mathbf{P}_2 = \nabla P_2(x, y, z)$**

We compute the *code of conduct payoff* (Figure 10-5), and see that it is quite different from the "Blue" and "Red" behaviors; however the engagement of the *code of conduct player* in this solution is small. The *composite payoff vector* (Figure 10-6) is primarily along the $z$ direction. This is the only direction that the two players have in common. The vector field is not uniform however, indicating the important effect of the various contributions. The effect of the outcome gauge field can be important, though not in the present case. We can have an initial vorticity, which through the field equations for the *characteristic potential* (section 8.12, exercise 14), will generate an influence.

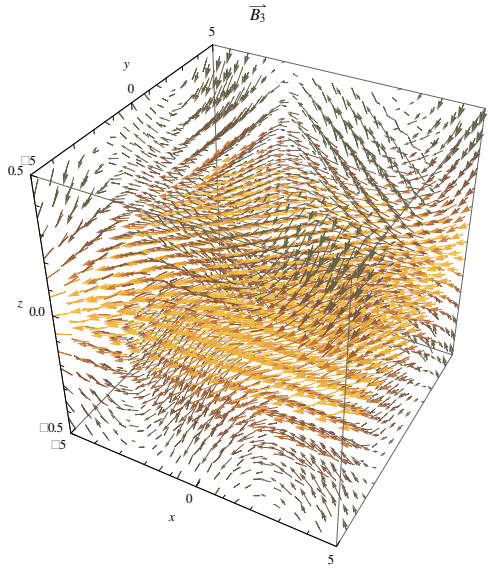


**Figure 10-5: Code of conduct payoff $\mathbf{B}_3$**

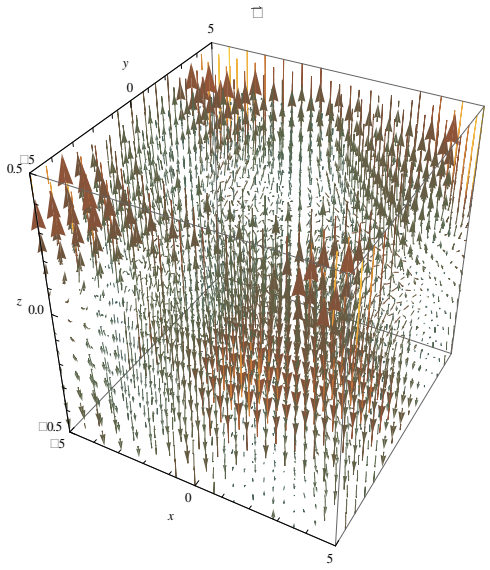


**Figure 10-6: *Composite payoff* field ω**

## 10.2 *Player interest*

To obtain the locked behavior, section 9.2, we have chosen large values for certain components of the *strategy bias field* $f^{j}{}_{ov}$:

$$\begin{aligned} I_{x\alpha}(0,0,0) &= \{-0.03054179...,-0.019419...,0\} \\ I_{y\alpha}(0,0,0) &= \{-0.0357018...,-0.0230003...,0\} \\ I_{z\alpha}(0,0,0) &= \{8.08112...,-7.861099...,0.301707...\} \end{aligned} \tag{10.2}$$

The other components are determined by using the observed payoff matrix to compute the observed player strategy bias, Eq. (8.51) in terms of the exact frame transformation $\left\{E^{a}{}_{v} \quad E^{a}{}_{o}\right\}$, Eq. (9.5).

This gives the contour plots for each player (Figure 10-7 and Figure 10-8) that have little structure. We have used Eq. (8.54) to solve these equations for the unknowns $I_{v\alpha}$, $\omega_{v\alpha\beta}$ and $e_3$ (since we assume $q_v = e_1 = e_2 = 0$). In the process we have made the following additional assumptions:

$$\begin{aligned} &\omega_{z11} = 4/10; \omega_{z22} = 5/10; \omega_{z33} = 6/10; \omega_{z12} = 0 \\ &I_{x3} = I_{y3} = 0 \end{aligned} \tag{10.3}$$

The boundary conditions at $z = 0$ have constraints to which we have conformed. For example, we have conformed the behavior of $I_{x\alpha}(x, y, 0)$ and $I_{y\alpha}(x, y, 0)$ to Eq. (8.29) in terms of the charge gradients and known boundary conditions.

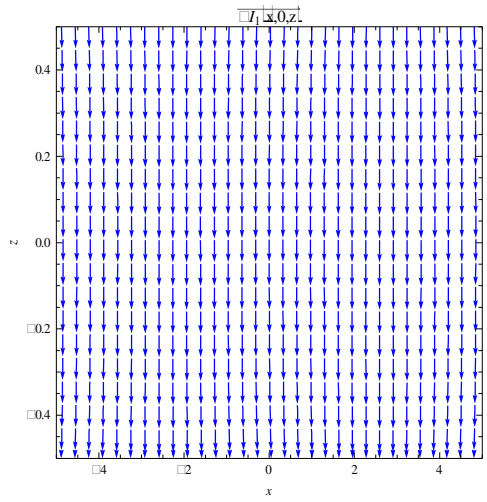


**Figure 10-7: "Blue" player interest** $\left\{\mathbf{I}^{\mathbf{x}}{}_{\mathbf{1}}(x,0,z)\quad \mathbf{I}^{\mathbf{z}}{}_{\mathbf{1}}(x,0,z)\right\}$

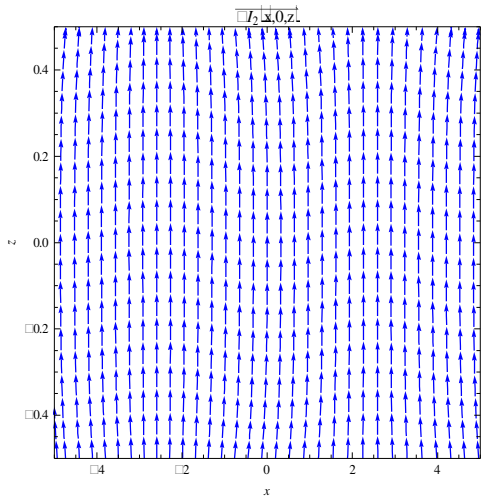


**Figure 10-8: "Red" player interest** $\left\{\mathbf{I}^{\mathbf{x}}{}_{\mathbf{2}}(x,0,z)\quad \mathbf{I}^{\mathbf{z}}{}_{\mathbf{2}}(x,0,z)\right\}$

In the player interest plots, we see a strong and opposite flow for each, indicating the effect of the added *player bias fields*.

## 10.3 *Shear, compression and payoffs*

We can decompose the components of the symmetric tensor $\omega_{\upsilon\alpha\beta}$ for each proper strategy $\upsilon$ into shear (a traceless matrix) and compression (the trace of the symmetric tensor), Eq. (8.18). These components determine payoffs that we can identify with cooperation and opportunity. We use the *known behavior* payoffs to set some of these values in Eq. (8.62). However, we have an insufficient set of data to complete the determination. We supplement our knowledge with constraints from the theory.

In addition to setting the initial values of $\omega_{\upsilon\alpha\beta}$, we must insure that the values are derived from a potential and that for each active proper strategy $\upsilon$, the matrices in the inactive index commute. Our approach is to separate out the compression $\Theta$ and the shear components $\sigma_{\upsilon\alpha\beta}$, using the above techniques for setting the initial values. We then iterate our process as follows. The components of $\sigma_{z\alpha\beta}$ are known with the exception of $\left\{\omega_{x11}\quad \omega_{x12}\quad \omega_{x22}\quad \omega_{y11}\quad \omega_{y12}\quad \omega_{y22}\right\}$. Given these values, all of the components of $\sigma_{z\alpha\beta}$ are known. Transform this matrix to a frame in which it is diagonal. Take for the diagonal shear matrix $\bar{\sigma}_{\alpha\beta}(x,y,0)$ a function that depends on six variables, assuming two variables for each diagonal component with each variable representing a degree of freedom along either $x$ or $y$. Take a form for $\partial_z\bar{\sigma}_{\alpha\beta}(x,y,0)$. It should be determined. Compute $\sigma_{x\alpha\beta}$ and $\sigma_{y\alpha\beta}$. This gives new values for the above unknowns, possible changing the value of $\sigma_{z\alpha\beta}$. This process can be iterated to closure.

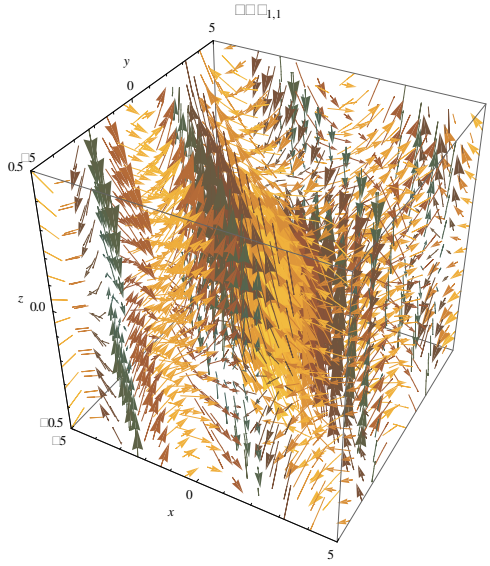

**Figure 10-9: Shear gradient** $\sigma^{v}{}_{11}$

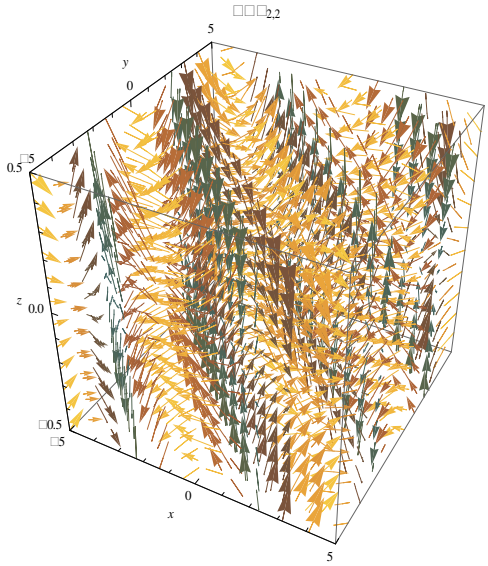

**Figure 10-10: Shear gradient** $\sigma^{v}{}_{22}$

We obtained closure with these *known behavior* values for the shear components:

$$\begin{aligned}
\sigma_{11}(x,y,0) &= 0.21111...\cos\frac{\pi y}{5}\sin\frac{\pi x}{5} + 0.19896...\cos\frac{\pi x}{5}\sin\frac{\pi y}{5} \\
\sigma_{12}(x,y,0) &= -0.14362...\cos\frac{\pi y}{5}\sin\frac{\pi x}{5} - 0.13499...\cos\frac{\pi x}{5}\sin\frac{\pi y}{5} \\
\sigma_{13}(x,y,0) &= -0.06050...\cos\frac{\pi y}{5}\sin\frac{\pi x}{5} - 0.05844...\cos\frac{\pi x}{5}\sin\frac{\pi y}{5} \\
\sigma_{22}(x,y,0) &= -0.41646...\cos\frac{\pi y}{5}\sin\frac{\pi x}{5} - 0.39142...\cos\frac{\pi x}{5}\sin\frac{\pi y}{5} \\
\sigma_{23}(x,y,0) &= -0.03433...\cos\frac{\pi y}{5}\sin\frac{\pi x}{5} - 0.03188...\cos\frac{\pi x}{5}\sin\frac{\pi y}{5} \\
\sigma_{33}(x,y,0) &= 0.20534...\cos\frac{\pi y}{5}\sin\frac{\pi x}{5} + 0.19246...\cos\frac{\pi x}{5}\sin\frac{\pi y}{5}
\end{aligned} \tag{10.4}$$

These shear components are zero at the *still point*.

As part of this process we also obtain the shear gradients along the $z$ axis:

$$\begin{aligned}
\sigma_{z\alpha\beta}(x,y,0) &= \begin{pmatrix} -1/10 & 0 & 0.29036... \\ 0 & 0 & -0.07259... \\ 0.29036... & -0.07259... & 1/10 \end{pmatrix} \cos^2\frac{\pi x}{10}\cos^2\frac{\pi y}{10} \\
\Theta(x,y,0) &= 0 \\
\Theta_z(x,y,0) &= -3/2\cos^2\frac{\pi x}{10}\cos^2\frac{\pi y}{10}
\end{aligned} \tag{10.5}$$

These shear components then generate the complex interplay of effects that we see in the figures. In Figure 10-9, we see the diagonal component for "Blue". We compare this with Figure 10-10 for "Red". They are similar though opposite in sign horizontally, but "Red" has no vertical component initially.

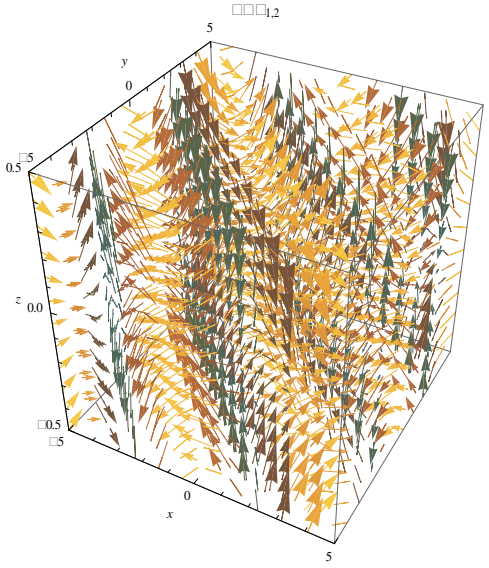

**Figure 10-11: Shear component $\sigma^{v}{}_{12}$**

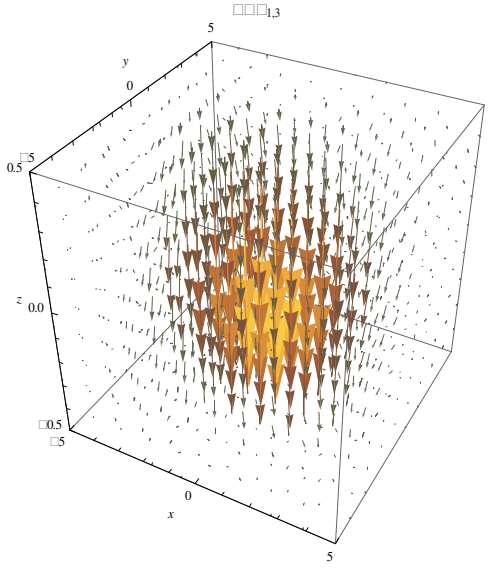

**Figure 10-12: Shear component $\sigma^{v}{}_{13}$**

The shear components for off-diagonal components are quite different.

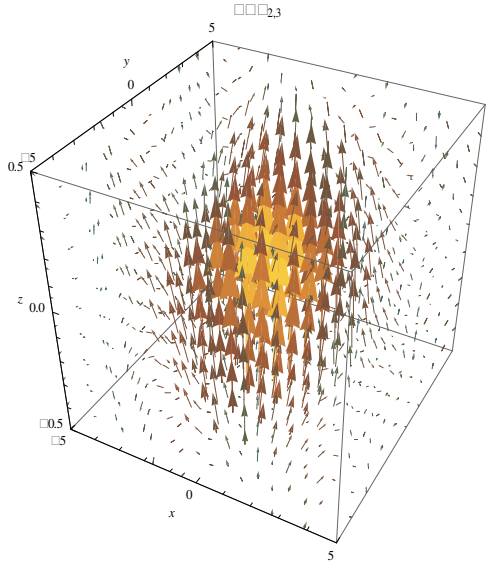

**Figure 10-13: Shear component $\sigma^{v}{}_{23}$**

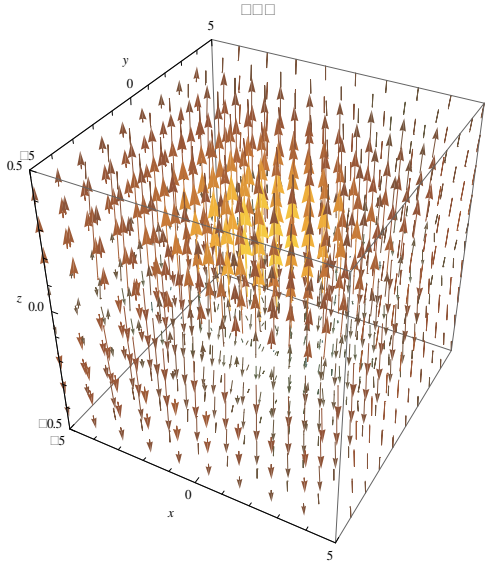

**Figure 10-14: Compression gradient $\Theta^{v}$**

Between the two players, Figure 10-11, the vector field is reasonably well spread out, whereas between "Blue" and the institutional player, Figure 10-12, the field is localized near the origin. We see something similar between the institutional player and "Red", Figure 10-13. There is also some localization of the compression gradient, Figure 10-14.

## 10.4 *Characteristic vector potential*

The *composite payoff* is determined not just by the *engagement* and *entitlement*, but also by the ***characteristic payoff*** via the ***characteristic vector potential***, Eq. (8.30). The *characteristic potential* is a vector field determined by Eq. (8.31), the gauge condition Eq. (4.136) and an additional condition on the boundary, section 8.12, exercise 14 and Eq. (8.75). The equations have a great many terms so it is helpful to identify ways that insure that the calculations are correct; using the fact that the two gauge condition should remain satisfied at all values of $z$ is one helpful check.

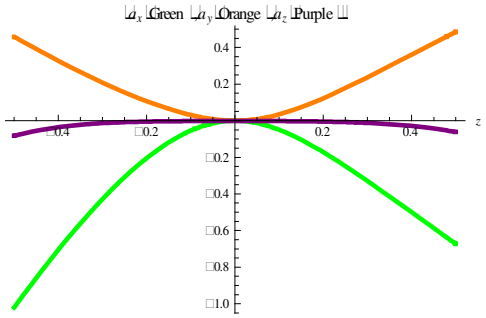


**Figure 10-15: Characteristic potential field** $a_v(0,0,z)$

We mentioned that for our example, the *characteristic potential* contribution was not large near the *still point*. However, we are free to fix the initial *vorticity vector* at the still point, which initializes the *gauge field*.

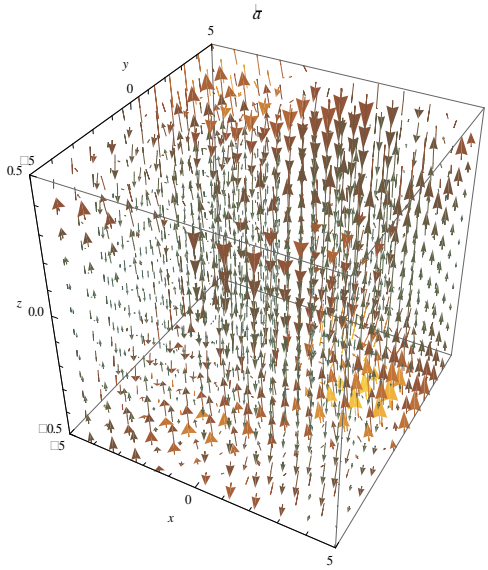


**Figure 10-16: Characteristic potential** $a_v$

For the cases shown, we have taken these initial values to be zero but have explored non-zero values and leave as an exercise to show that the effects can be large, even at the *still point*. The *characteristic potential* starts at zero at the *still point*. All the components become active, Figure 10-15 and Figure 10-16.

## 10.5 *Validity regions*

One very specific consequence of the theory is that not all values of the fields are meaningful. The analogy from physics is that not all speeds are possible. You can't go faster than the speed of light nor can the speed of light be zero. Such constraints are natural in a complete theory and resolve the problems in a natural way. You can't go faster than the speed of light arises because to go faster than that speed you would need sufficient energy. However the closer to the speed of light you get, the more energy it takes until you need all the energy in the universe to achieve your goal.

There are also constraints due to the coordinate system used. For example you can project the sphere onto a plane, yet the projection will have one point, the North Pole, that lies at infinity. This is an artifact of the coordinate system, not an intrinsic problem of the sphere. What it suggests is that you have to identify when you are getting close to singular points and determine whether they are artifacts of the coordinate system or the description.

We have suggested several lines of investigation in the exercises. For free fall behavior, in the last chapter, we considered the set of constraints imposed based on the properties of the frame transformations, section 9.5, exercise 20. The possible regions are highlighted in Figure 9-37.

In the exercises at the end of this chapter, we continue that analysis. For example, one constraint comes from causality, exercise 2. This also deals with the constraint that comes from the reasonable notion that volume elements that start off as non-zero should remain non-zero as they dynamically move. We can construct communication ellipsoids, exercise 3 that indicate how the effects due to an event can generate causality. The constraint is that the shape is an ellipsoid and this imposes constraints on the allowed values of some of the metric elements. These constraints in turn impose constraints on the behavior of the flows, exercise 5 and velocity streamlines exercise 6.

## 10.6 *Outcomes*

We have examined a large number of equations and a correspondingly large number of curves dealing with the attack-defense model. We have observed the effects of many mechanisms such as *player interest*, *engagement*, *entitlement*, *passion*, and *strategy bias.* We observe that they play as big a role in *decision process theory* as do the concepts of *game values*, *payoffs* and *Nash equilibrium* that we take from *game theory*. These insights we believe can contribute to our understanding of decision processes. Our numerical computations can be modified to incorporate any other two-person game with two-strategies per player. We believe that such an extension significantly advances our understanding since we now deal with a very large number of games that have already been dealt with in the game theory literature. With effort we can also extend the discussion to games of three or more players or games in which each player has more than two strategies. In principle, our theory deals with any number of players who have any number of strategies.

We think it possible that Mathematica's *numerical method of lines* will provide practical solutions even with more players and more strategies, though we look forward to using the finite element method when it becomes available. If we extend our numerical efforts to differing numbers of players or strategies, what might we expect? As in *game theory*, the possibilities become even more interesting as we increase the number of players. For example, it is not a reach to extend our analysis to three-person processes as well as four player processes with active strategies $\{u_1 = r_1 - r_2 \quad u_2 = r_2 - r_3 \quad u_3 = r_3 - r_4\}$. We thus expect a more extensive discussion of which combinations of strategies are active and which are inactive and part of a code of conduct.

Even if the numerical calculations are difficult, we may still gain insight without performing the entire analysis. For example, in dealing with decision processes having three or more players, we have in common with *game theory* a new attribute that appears to be related to forming coalitions, (Von Neumann & Morgenstern, 1944, p. 220). Our discussion and conclusions are quite different however. For example with a decision process having three agents, assume that the inactive strategies are the *player relative preferences* $s_{jk}$ and the sum of the *player preference scales* $r_1 + r_2 + r_3$. The active strategies $\{u_1 = r_1 - r_2 \quad u_2 = r_2 - r_3\}$ provide non-zero ***observed player strategy bias*** fields $f^{j}{}_{o\, r_i + r_j}$ between players that are not possible with only two players. As in game theory, this appears to reflect a payoff based on a coalition between players as opposed to the *skill based payoffs*. However we need not introduce mechanisms such as *imputations* and *dominance* that have now fallen out of favor (*Cf.* section 7.3 and the quote from (Aumann, 1989, p. 13)): here, the field equations of *decision process theory* suffice. The only changes are those specific to identifying which strategies are active and which are inactive.

In addition to these general considerations, the student should have learned the following outcomes:

- The student should be able to speak differently about decision processes based on the introduced concepts such as *entitlement*, *engagement*, *passion*, and *player interest*.
- The player should understand dynamic payoffs and the sense in which they are generated from "currents" defined as the player passions. In a decision, actions are the result of the composite payoffs, not the passions or the individual payoffs.
- The student should understand the concepts of shear, compression and inertia and how they can be generated from the related concepts of passion and interest. These concepts determine the degree of cooperation in the decision process.
- The student should understand how the characteristic payoff represents the composite behavior of all of the agents involved in the decision process. These concepts determine the degree of competition in the decision process and how the competitive issues are resolved.

The attainment of the outcomes of this chapter is facilitated by doing the exercises in the following section.

## 10.7 *Exercises*

1. As a way to understand why these regions are excluded in section 9.5, exercises 19-20, derive the following equations. They show that the inverse frame transformation can be determined from a reduced spatial frame transformation $\tilde{E}^{u^m}_{\ v^n}$. To compute this, we require that $E^t_{\ o} \neq 0$ and the determinant $\left\| \tilde{E}^{u^m}_{\ v^n} \right\| \neq 0$ is non-singular.

$$\tilde{E}^{u^m}_{\ v^n} = E^{u^m}_{\ v^n} - \frac{E^{u^m}_{\ o} E^t_{\ v^n}}{E^t_{\ o}}$$

$$\tilde{E}_{u_m}^{\ v^n} \tilde{E}^{u^l}_{\ v^n} = \delta^l_m$$

$$(-)^{n_a} \left\| g^{ab} \right\| = \left(1 + e_\alpha e^\alpha\right) \left\| \begin{matrix} E^{u^m}_{\ v^n} & E^{u^m}_{\ o} \\ E^t_{\ v^n} & E^t_{\ o} \end{matrix} \right\|^2 = \left(1 + e_\alpha e^\alpha\right) \left(E^t_{\ o}\right)^2 \left\| \tilde{E}^{u^m}_{\ v^n} \right\|^2 \qquad (10.6)$$

$$\begin{pmatrix} E^{v^m}_{\ u^n} & E^{v^m}_{\ t} \\ E^o_{\ u^n} & E^o_{\ t} \end{pmatrix} = \begin{pmatrix} \tilde{E}^{v^m}_{\ u^n} & -\frac{\tilde{E}^{v^m}_{\ u^l} E^{u^l}_{\ o}}{E^t_{\ o}} \\ -\frac{E^t_{\ v^l} \tilde{E}^{v^l}_{\ u^n}}{E^t_{\ o}} & \frac{E^t_{\ o} + E^t_{\ v^l} \tilde{E}^{v^l}_{\ u^i} E^{u^i}_{\ o}}{E^t_{\ o} E^t_{\ o}} \end{pmatrix}$$

2. Using Eq. (10.6), comment on these proposed rules that must be satisfied by sensible solutions using the harmonic gauge coordinates to evaluate the frame transformations:

   - The causality assumption: $\frac{dt}{d\tau} = E^t_{\ o} > 0$. Along the streamline, the proper time must increase: $\tau > 0$, so this says that along the streamline in any frame given by the harmonic gauge, time must strictly increase.
   - For $n_a$ active strategies, the invariant volume element $\int \sqrt{|g|} du^1 \wedge \ldots \wedge du^{n_a} \wedge dt$ is used to define the action, Eq. (2.29). The measure is non-singular so the determinant $0 < \left| g^{-1} \right| < \infty$. The consequence for the harmonic gauge is that the frame transformation matrix is non-singular. In the model I have been using, the determinant $\left\| g^{ab} \right\|$ can be factored into a proper charge factor $\left(1 + e_\beta e^\beta\right)$ and the square of the frame determinant $\left\| \begin{matrix} E^{u^m}_{\ v^n} & E^{u^m}_{\ o} \\ E^t_{\ v^n} & E^t_{\ o} \end{matrix} \right\|$. Here $1 \le m, n \le 3$ for the numerical computations. The frame determinant can be written as $E^t_{\ o} \left\| E^{u^m}_{\ v^n} - \frac{E^{u^m}_{\ o} E^t_{\ v^n}}{E^t_{\ o}} \right\|$, so the new condition is that the reduced determinant is non-singular: $\left\| \tilde{E}^{u^m}_{\ v^n} \right\| > 0$. Note that we make use of the fact that $E^t_{\ o} > 0$.
   - In any frame, the time component of the energy momentum tensor $T_{tt}$ is the energy and should be positive. It can be written in terms of the energy density $\mu$ by use of the frame

transformations: $T_{tt} = \mu E_t^{\ o} E_t^{\ o}$. If you start in a regime in which $E_t^{\ o} > 0$, argue that the energy can't change sign, hence this condition stays valid everywhere.

3. The following argument puts a tighter bound on $E_t^{\ o}$. The argument is certainly plausible but is it correct? Discuss. Through each point along a streamline, consider the null geodesics, which satisfy Eq. (10.7). We can insure that $g_{tt} > 0$ at some initial point along the streamline. At each point along the streamline, the equation describes an ellipsoid shape determined by the eigenvalues of the spatial components of the metric and the off-diagonal time term. The eigenvalues $\overline{g}_{mm}$ are assumed to be non-zero, which is true as long as $\left\| g_{mn} \right\| = g g^{tt} \neq 0$. We assume $E^t_{\ o} > 0$ and $\left\| \tilde{E}^{u^m}_{v^n} \right\| > 0$ so we also must have $g^{tt} > 0$. As examples of the ellipsoid, we show two cases: one with $g_{tt} > 0, \quad g^{tt} > 0$ and one with $g_{tt} > 0, \quad g^{tt} < 0$. In both cases $E^t_{\ o} > 0, \quad E_t^{\ o} > 0$. The values are computed from the model displayed in Figure 9-36 and Figure 9-37 with $\tau = 1, \quad z = 0$ and $-0.2$ respectively.

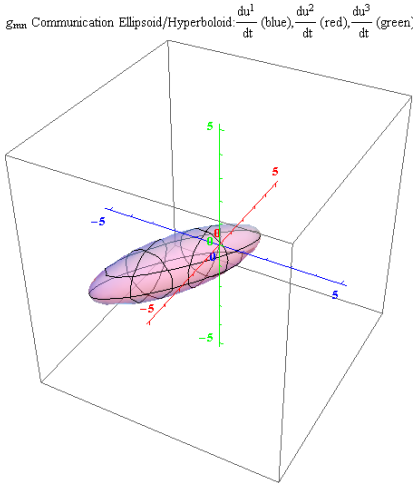


**Figure 10-17: Communication ellipsoid** $g_{tt} > 0, \quad g^{tt} > 0$

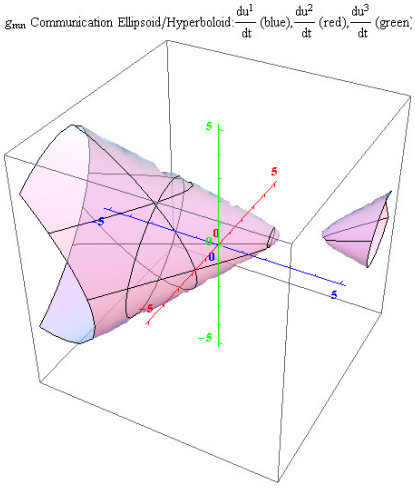


**Figure 10-18: Communication hyperboloid** $g_{tt} > 0, \quad g^{tt} < 0$

We see that when $g^{tt} > 0, \quad g_{tt} > 0$, the shape is a ***communication ellipsoid***, which implies that at each point, there is an open set around the streamline and there is a null flow in any direction in that open set. If along the streamline one of the eigenvalues $\overline{g}_{mm}$ goes to zero, then $g^{tt} = 0$ and from Eq. (10.7), the shape is no longer an ellipsoid.

$$g_{ab} \frac{du^a}{dt} \frac{du^b}{dt} = 0 \Rightarrow g_{mn} \frac{du^m}{dt} \frac{du^n}{dt} + 2 g_{tm} \frac{du^m}{dt} + g_{tt} = 0$$

$$\overline{g}_{mm} \dot{\bar{u}}^m \dot{\bar{u}}^m + 2 \overline{g}_{tm} \dot{\bar{u}}^m + g_{tt} = 0 \qquad (10.7)$$

$$\left\| g_{mn} \right\| \neq 0 \Rightarrow -\sum_m \overline{g}_{mm} \left( \dot{\bar{u}}^m + \overline{g}_{tm} \overline{g}_{mm}^{\ -1} \right)^2 = -\sum_m \overline{g}_{tm} \overline{g}_{mm}^{\ -1} \overline{g}_{mt} + g_{tt}$$

The shape, a ***communication hyperboloid***, in general is unbounded (Figure 10-18), suggesting that for some direction, "light" can travel with infinite speed. This suggests the condition $g^{tt} > 0$.

Assuming this condition, when $g_{tt}=0$, the *communication ellipsoid* (or *communication hyperboloid*) passes through the point in which every eigen-velocity $\dot{\bar{u}}^m$ is zero. We consider $g_{tt}=0$ to be a singular point, since this means that for an open set around that point on the streamline, there will be parts of space that will never be reached. It seems reasonable that you should be able to communicate to any part of space, so $g_{tt}>0$, which ensures that zero velocity $\forall m=1,2,3:\dot{\bar{u}}^m=0$ occurs strictly inside the ellipsoid. In physics we have black holes in which light can enter but not escape in certain directions. Does this mean that these conditions are too strong, or simply that we have identified the singular points?

4. We make a similar argument using the covariant flows. Though plausible, is this argument correct? Consider the invariant energy momentum flow for "light" $g^{ab}\pi_a\pi_b=0$ at each point along the streamline. The argument proceeds exactly as in the previous exercise. Here we would argue that $g_{tt}>0$ to ensure a bounded shape for the *covariant communication ellipsoid*. If we further allow the possibility that $g^{tt}=0$ at some point along the streamline, then again it appears that light gets trapped. This is a contradiction so we have the additional condition that $g^{tt}>0$ and the origin is inside the ellipsoid.
5. To give a picture to the possible topological shapes, consider the figures below for a two harmonic model in which in one case we have a weaker-amplitude and the other a stronger-amplitude.

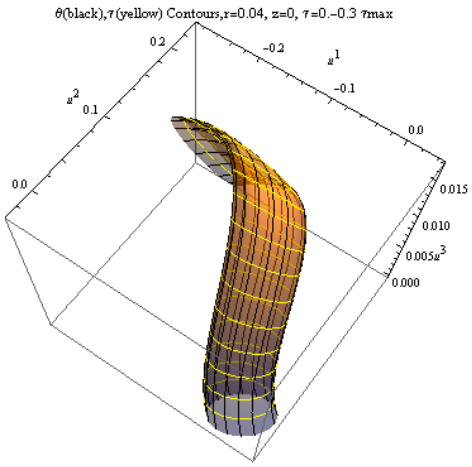


**Figure 10-19: Two harmonic model, weak amplitude**

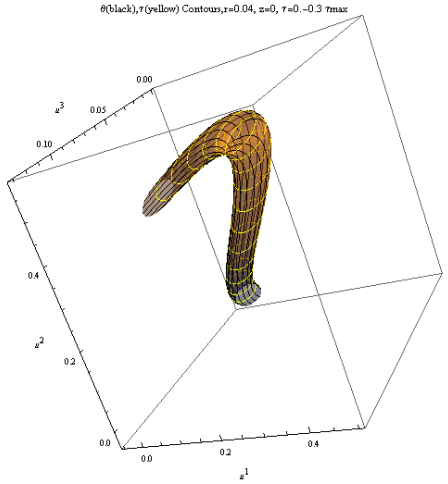


**Figure 10-20: Two harmonic model, strong amplitude**

Note that for the weak amplitude, Figure 10-19, the streamlines go around the bend. They don't touch. For the strong amplitude, Figure 10-20, as the streamlines go around the bend, the outside becomes the inside and the inside becomes the outside. The streamlines do touch. What is the physical meaning of this reversal? Though plausible, it does not correspond to a singularity of $g_{tt}$ .

6. Investigate the effects of $g^{tt}$ vanishing by considering a model in which only the time components has three harmonics and where for each of the space directions, a single free fall harmonic. Show that for strong amplitude, the shape of a tube of velocity streamlines has the same shape as the free fall solution, Figure 10-21.

7. Show that the velocity of the ***normal-form coordinate basis*** as seen in the ***co-moving coordinate basis*** is characterized as the ***now-β***: $\beta_\upsilon = E^t{}_\upsilon \big/ E^t{}_o \sqrt{1+e^\alpha e_\alpha}$ . This is the velocity of the coordinate time surface: i.e. "now". Show that this is obtained from the normal-form coordinate time surface $t(x)$ whose normal to the surface is $\partial_\mu t = \delta_\mu{}^t$ . Transform this covariant vector to the co-moving coordinate basis. This velocity must be strictly less than unity, since we assume that they travel strictly less than the speed of communication ("light"). We say that two frames are ***communication compatible*** if we can move from one frame to another at less than light speed.

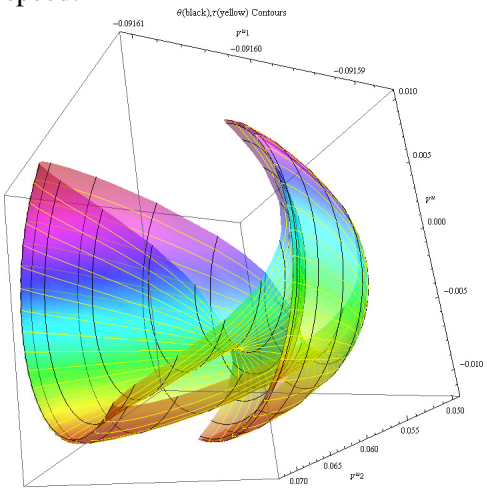


**Figure 10-21: Velocity streamlines with three harmonics**

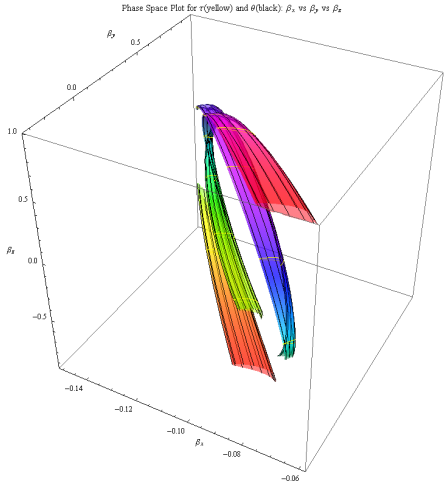


**Figure 10-22: For the three harmonic model, the β plot**

8. As a continuation of the investigation of the requirement that $g^{tt} > 0$, show that this is a requirement on the normal to the "time" coordinate plane. In particular, in the orthonormal rest frame, the normal is the vector $\{E^t{}_o \quad E^t{}_\alpha \quad E^t{}_\upsilon\}$ and the velocity vector can be thought of as the *now-β*, Exercise 7: $\boldsymbol{\beta} = \{\beta_x \quad \beta_y \quad \beta_z\}$. The constraint is that $|\boldsymbol{\beta}| < 1$ and is illustrated in Figure 10-22, with $r = 0.2 \quad z = 0.1$. A gap in the streamline is when this constraint is not met.
9. The *now-β* of Exercise 7 is determined by the covariant component of the 1-form $\mathbf{X} = X_\mu du^\mu$ for the special case in which $X_\mu = \delta_\mu{}^t$ is along the time direction. The 1-form is the line element that moves along the normal to the time surface: we have ***normal time***. The use of the word "normal" assumes we have a meaning of what it means to be at right angles. We have other ways to define "normal": the *metric* and *forms*. Consider the vector $Y^\mu = \delta^\mu{}_t$ . We construct the $n-1$ form from all the space components which is a hypersurface and another candidate for "normal": $\mathbf{Y} = Y^\mu \varepsilon_{\mu 1 \cdots n_a} du^1 \wedge \cdots \wedge du^{n_a}$, using the fully anti-symmetric tensor $\varepsilon$. The component vector $Y^\mu$ represents a vector that is along the "normal" to the surface defined by the antisymmetric hypersurface form. It is orthogonal to the space components: we have ***orthogonal time***. In the co-moving orthonormal basis, the components are $\{E_t{}^o \quad E_t{}^\alpha \quad E_t{}^\upsilon\}$ and define a dual velocity ***now-*β***: $^*\beta^\upsilon = E_t{}^\upsilon \big/ E_t{}^o \sqrt{1+e^\alpha e_\alpha}$ . Using the condition $g_{tt} > 0$ and the definition of the metric in terms of the frame transformation, show that this means $|^*\boldsymbol{\beta}| < 1$. This says that both

definitions of "normal" make sense and that each vector, the *now-β* and its dual *now-*β*, must be less than unity. If we start with that principle we arrive again at the conditions $g^{tt} > 0$ and $g_{tt} > 0$ respectively. Show that the two velocities, which may be equal at one point, are not in general equal, as shown in the figures below. Show that the n-form $\mathbf{X} \wedge \mathbf{Y}$, which is the wedge product of the two forms, does not vanish. Show that the product of the components is $X_\mu Y^\mu = 1$. Show that the product of the two velocities is: $*\beta^\upsilon \beta_\upsilon = \frac{E_t{}^\upsilon E^t{}_\upsilon}{\left(1+e^\alpha e_\alpha\right) E_t{}^o E^t{}_o} = \frac{1}{\left(1+e^\alpha e_\alpha\right) E_t{}^o E^t{}_o} - 1$.

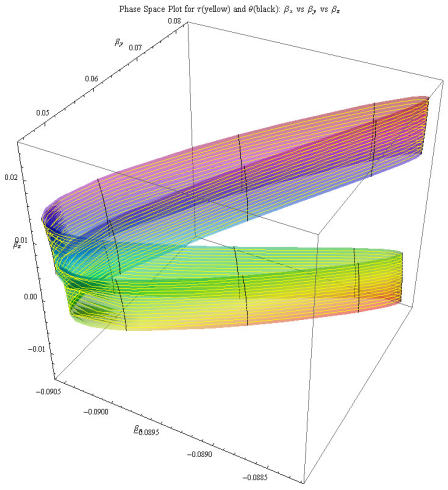


**Figure 10-23: Now-β for the two-harmonic model along u**

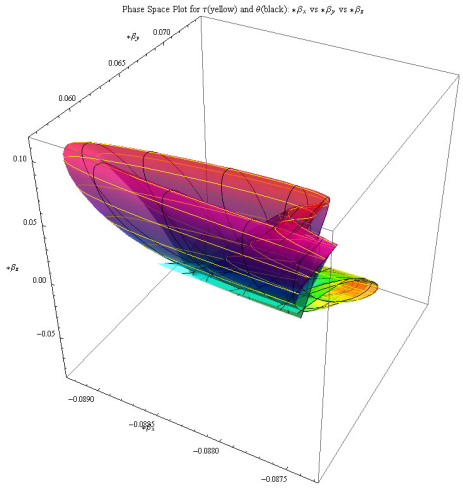


**Figure 10-24: Now-*β for two harmonic model along u**

10. It may seem strange to associate a velocity with an n-form. However, recall that fluid flow consists of the amount of energy in a differential volume: see for example Eq. (2.7). Thus the ***flow-β***, defined as $\beta^{u^m}{}_{flow} = E^{u^m}{}_o \Big/ E^t{}_o E_t{}^o \sqrt{1+e^\alpha e_\alpha}$, should be related to the dual now-*β. To support this definition, show that the flow-**β** is a rotation of the dual-***β**:

$$E_t{}^o \sqrt{1+e^\alpha e_\alpha}\,\beta^{u^m}{}_{flow} = -\frac{*\beta^{\upsilon^n} E^{u^m}{}_{\upsilon^n}}{\sqrt{1+e^\alpha e_\alpha}\,E^t{}_o} = -*\beta^{\upsilon^n} \tilde{E}^{u^m}_{\upsilon^n} \sqrt{1+e^\alpha e_\alpha}\,E_t{}^o \qquad (10.8)$$

$$\beta^{u^m}{}_{flow} = -*\beta^{\upsilon^n} \tilde{E}^{u^m}_{\upsilon^n}$$

11. Show that the flow-β is bounded: $\left|\boldsymbol{\beta}_{\mathbf{flow}}\right|^2 < \chi^2$. Use Eq. (10.6) and the fact that the dual *now-*β* is bounded by unity. Can you determine $\chi$?
12. Based on the Exercises 7-11, show that the frame transformation is characterized by the *now-β,* the dual *now-*β*, the time flow $E^t{}_o$ and the reduced frame transformation matrix $\tilde{E}^{u^m}_{\upsilon^n}$, Eq. (10.6).